Robotics and Computer Integrated Manufacturing 53 (2018) 58–71

Contents lists available at ScienceDirect

Robotics and Computer Integrated Manufacturing

journal homepage: www.elsevier.com/locate/rcim

A new methodology for joint stiffness identification of heavy duty industrial robots with the counterbalancing system

Kun Yang[a,b], Wenyu Yang[b,*], Guangdong Cheng[b], Bingrong Lu[c]

[a] School of Material Science and Engineering, Huazhong University of Science and Technology, Wuhan 430074, China
[b] State Key Laboratory of Digital Manufacturing equipment and Technology, School of Mechanical Science and Engineering, Huazhong University of Science and Technology, Wuhan 430074, China
[c] Huaheng Weld Co., Ltd., Kunshan 215347, China

ARTICLE INFO

Keywords:
Joint stiffness identification
Heavy duty industrial robot
CBS
Current

ABSTRACT

This paper deals with the joint stiffness modeling and identification of the heavy duty industrial robot with the counterbalancing system (CBS), which is important for the workspace optimization and deflection compensation in the robotic manufacturing. Shortcomings of the traditional method for the joint stiffness modeling and corresponding identification are analyzed in this paper. Motivated by the advantage and limitations of the traditional approach, a new identification methodology based on the servo motor current and corresponding position deflection is proposed to obtain the accurate joint stiffness. To validate the effectiveness of the proposed method for the joint stiffness modeling and identification, an identification and validation experiment is carried out using the HH-150 heavy duty industrial robot. The results show that the proposed methodology is able to identify the joint stiffness of the heavy duty industrial robot with the CBS, and the proposed new methodology outperforms in terms of accuracy, convenience and efficiency for the joint stiffness identification.

1. Introduction

Owing to the low investment and high production flexibility, recent studies have demonstrated that heavy duty industry robots are gradually becoming more competitive than the CNC machine in the manufacturing industry, such as grinding [1], boring [2], machining [3,4] and the friction stir welding (FSW) [5]. Because of high forces generated in these applications, the insufficient stiffness of robots becomes the main obstacle for high-accuracy robotic manufacturing applications [4,6]. Especially for the machining and FSW process, the process load would make the joint deform, and the deflection is produced at the end of the manufacturing tool, degrading the quality of the final product [7]. One possible way to solve this problem is to optimize the workspace or compensate the deflection based on the robot stiffness [6,8]. To implement this approach, an accurate stiffness modeling of heavy duty industrial robot as well as the corresponding stiffness identification plays an important role in the robotic manufacturing process [9], which is the main focus of this paper.

The robot stiffness describes the manipulator resistance to the deformation caused by the external force/torque applied to the end-effector (EE). Usually, the characteristic of the robot stiffness is numerically defined as a Cartesian stiffness matrix, which represents a linear relation between the translational/rotational displacement and force/torque in the EE. Similarly, the joint stiffness denotes the relation between the force/torque and corresponding deflections in the joints. In general, methods for the robot stiffness modeling are roughly divided into three groups: the Finite Elements Analysis (FEA), the Matrix Structure Analysis (MSA), and the Virtual joint method (VJM) [10]. The basic principle of the FEM method is to decompose the physical model of the structure on a number of finite elements and to introduce compliant relations between adjacent nods described by relevant stiffness matrices. As it considers the true shape and dimensions of the robot, the FEM method seems to be the most accurate one for the stiffness modeling [11]. Nevertheless, due to the high computational efforts and numerous accumulative round-off errors, this method is usually applied at the design stage [12]. To overcome the high computational effort, the MSA method is proposed to obtain the stiffness matrix by using beams, arcs and cables instead of complex links [13]. However, this simplification inevitably reduces the modeling accuracy. Meanwhile, the factor of assembling is also the key contribution of the stiffness matrix, and it cannot be accurately modeled by these two methods. The VJM method deals with the robot stiffness based on the extension of the traditional rigid-body model by adding virtue joints (localized springs), where links are regarded as rigid while the joints are assumed to be

* Corresponding author.
E-mail address: mewyang@hust.edu.cn (W. Yang).

https://doi.org/10.1016/j.rcim.2018.03.001
Received 12 September 2016; Received in revised form 6 January 2018; Accepted 1 March 2018
Available online 26 March 2018
0736-5845/

compliant [9,14,15]. This method provides reasonable trade-off between the model accuracy and identified complexity, and it will be used for the stiffness modeling in this paper.

Salisbbury [16] and Gosselin [17] are the first researchers to introduce the VJM method for the robot stiffness analysis. In their studies, the main compliance of the robot is assumed to be concentrated in the joints, and the mapping of stiffness matrices between the Cartesian and joint spaces is put forward. Later, Chen and Kao [18] reported that the conventional formulation derived by Salisbbury was not valid and a new conservative congruence transformation was used as a generalized relationship between the joint stiffness matrix $\mathbf{K}_{\boldsymbol{\theta}}$ and Cartesian stiffness matrix $\mathbf{K}_{\mathbf{X}}$. Based on this study, an enhanced stiffness modeling, identification and characterization for robot manipulators is proposed by Alici [19]. For the enhanced model, a complementary stiffness matrix $\mathbf{K}_{\mathbf{c}}$ is added in the conventional stiffness model by considering the external load and robot configuration. Subsequently, Dumas [20,21] proposed a robust procedure for the joint stiffness identification of the industrial robot based on the analysis of the complementary matrix $\mathbf{K}_{\mathbf{c}}$. Recently, Klimchik [9] proposed a sophisticated stiffness model based on the VJM method, which takes into account flexibilities of all mechanical elements.

To enhance the stiffness and payload capability of the heavy duty industrial robot, manufacturers tend to increase the link cross-section that inevitably leads to the augmentation of the robot mass. As a result, the second joint always bears the worst load during heavy duty applications. Therefore, the CBS is usually applied to minimize the torque in the second joint, which considerably complicates the stiffness modeling and identification. However, the problem of joint stiffness modeling for the robot with CBS has been rarely reported in current researches. One of the relevant works is devoted to regarding the CBS as an equivalent virtual spring [22,23]. In this study, the equivalent stiffness of the CBS is identified simultaneously with the joint stiffness. Nevertheless, the classical method for the joint stiffness identification is performed by the measurement of applied loads and corresponding deflection of the EE. In this way, it may be impossible to accurately obtain the spring stiffness, as the influence of the CBS on the second joint is almost eliminated by the comparison of these two robot states, before and after loading (namely, the influence of the CBS before loading is almost the same as that after loading). Besides, for the heavy duty industrial robot, such as Kuka KR-500MT and HH-150 (self-developed by Huaheng Weld Co., Ltd), the CBS is composed of the hydro-pneumatic system, and it is not reasonable to simplify the CBS to the virtual spring. To improve the modeling and identification accuracy of the CBS, a new methodology reflecting the clear physical meanings of the CBS is proposed in this paper.

Apart from the stiffness modeling and identification of the CBS, the traditional method for the joint stiffness identification has several shortcomings, which is assumed that the applied loads measured by the force sensor is the sole factor for the joint deformation. Actually, the practical force contributing to the deflection after loading is not the same as the measurement of the force sensor. Meanwhile, positions of three more reference points are required to obtain the orientation deflection, causing the placement error of the measurement system under each joint configuration. And the detailed problem for the joint stiffness modeling and identification of the heavy duty industrial robot is stated in Section 3.

Motivated by the advantage and limitations of the current research, a new and more accurate methodology is proposed for the joint stiffness identification of the heavy duty industrial robot with the CBS. The main attention is paid to the new theoretical stiffness model and corresponding identification method. The content of this paper is organized as follows. In Section 2, the kinematic model of the heavy duty industrial robot with the CBS and the joint stiffness model are presented. Section 3 describes the study motivation, which is based on problems for the joint stiffness identification. A new methodology for the joint stiffness identification is proposed in Section 4. Section 5 describes the identification experiment and corresponding results of the HH-150 robot based on the proposed method. In Section 6, the experiment is carried out to validate the identified joint stiffness. Finally, Section 7 summarizes the main contribution of this paper.

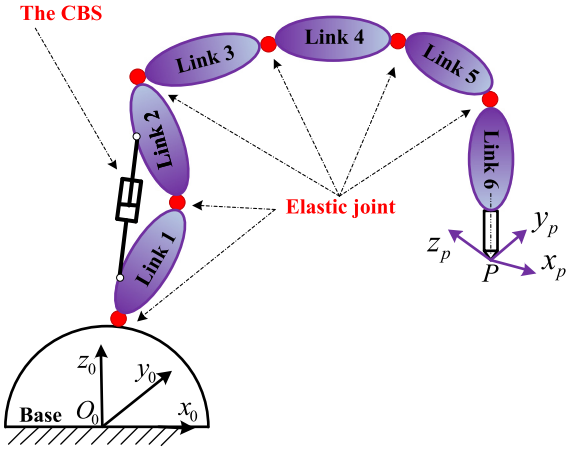

Fig. 1. The VJM model of the HH-150 robot.

2. Kinematics and joint stiffness modeling

2.1. Forward kinematics of the HH-150 robot

As illustrated in Fig. 1 and Fig. 2, the HH-150 robot can be represented as a sequence of rigid links separated by elastic joints based on the VJM model. Meanwhile, the CBS is attached to the first and second links, which generates the balancing torque for the second joint. When the robot is under heavy duty applications, the real joint position θ_i has two components: the command joint position and the deformed position caused by the force/torque [24].

$$\theta_i = q_i + \Delta\theta_i \tag{1}$$

Where q_i denotes the command joint position, and $\Delta\theta_i$ represents the deformation of the ith joint.

The CBS is a passive mechanism, whose kinematics is determined by the second joint variable θ_2. Thus, kinematics of the heavy duty industrial robot is only relative to the joint position vector $\boldsymbol{\theta}$, and all issues related to kinematics are identical to those of the conventional rigid robot [24]. In this case, the transformation between each two adjacent links is defined as

$$\mathbf{T_i} = \mathrm{Rot}(x, \alpha_{i-1})\mathit{Trans}(a_{i-1}, 0, 0)\mathrm{Rot}(z, \theta_i)\mathit{Trans}(0, 0, d_i) \tag{2}$$

Where $\mathbf{T_i}$ is the homogenous matrix representing the transformation of the ith link frame to the $i-1$ th link frame, and the details of the

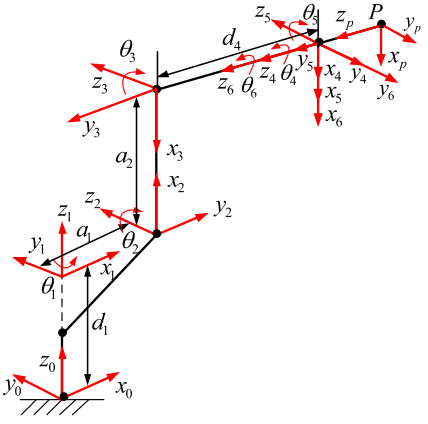

Fig. 2. D-H parameters of HH-150 robot.

Table 1
D-H parameters of the HH-150 robot.

Link i	a_{i-1}	α_{i-1}	d_i	θ_i	Parameters
1	0	0°	d_1	θ_1(0°) (± 185°)	
2	a_1	− 90°	0	θ_2(−90°) (−40–110°)	a_1 = 350 mm a_2 = 1200 mm d_1 = 683 mm d_4 = −1049 mm
3	a_2	0°	0	θ_3(180°)(−190–54°)	
4	0	− 90°	d_4	θ_4(0°) (± 350°)	
5	0	90°	0	θ_5(0°) (± 120°)	
6	0	− 90°	0	θ_6(0°) (± 350°)	

other parameters are obtained according to the classical D-H method [25].

Hence, the forward kinematics of the HH-150 robot considering elastic joints and the CBS is written as

$$\mathbf{T}=\mathbf{T_1T_2T_3T_4T_5T_6T_{tool}} \tag{3}$$

Here, $\mathbf{T_{tool}}$ denotes the transformation of the reference point relative to the last link frame. For further convenience, after extraction the rotation and translation components from the homogeneous matrix **T** [26], the kinematic model can be rewritten in a more conventional form

$$\mathbf{t} = (\mathbf{p},\ \varphi)^T = f(\theta,\ \mathbf{p_t}) \tag{4}$$

Where $\mathbf{p_t}$ is the pose vector of the reference point in the EE relative to the frame of the last link. The vector **t** defines the reference point position $\mathbf{p} = (x, y, z)^T$ and orientation $\varphi = (\phi_x, \phi_y, \phi_z)^T$ with respective to the base frame.

Therefore, once the joint deformation vector $\Delta\boldsymbol{\theta}$ is known, the real pose (position and orientation) of the reference point could be calculated through Eqs. (1) and (4).

2.2. Mechanics of the CBS

The mechanical structure of the CBS for HH-150 robot is presented in Fig. 3. The CBS consists of an accumulator, a hydraulic cylinder, a pressure gauge and an accumulator safety valve, which creates a closed and hydro-pneumatic loop. This design allows the CBS to generate the balancing torque smoothly to the second joint. In the case of the second joint rotating, the volume of gas in the accumulator is adjusted by the hydraulic oil. Then, the pressure is changed in the opposite direction

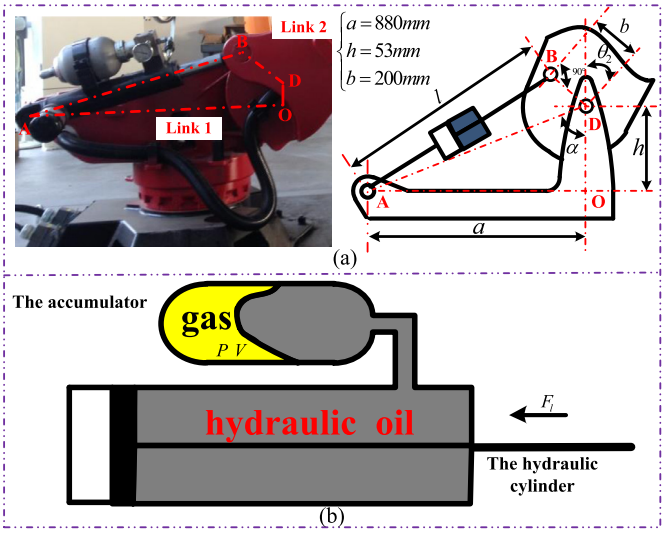

Fig. 3. The mechanics of the HH-150 robot: (a) The CBS of the robot, and (b) the working principle of the CBS.

compared to the volume of gas. As a result, the thrust force from the hydraulic cylinder is adjusted to balance the torque in the second joint.

When the volume of gas is changed with the rotation of the second joint, the pressure of the system satisfies the ideal gas law (namely, C is almost equal to constant).

$$P_iV_i = P_0V_0 = C \tag{5}$$

Assuming that P_0, V_0 are the initial gas pressure and volume when the piston rod of the cylinder is in the initial position, where the length of **AB** is equal to l_0. According to the force balance between the gas and hydraulic oil, the force F_l generated by the cylinder satisfies the following equation.

$$\frac{F_l}{F_{l_0}} = \frac{P_lS}{P_0S} = \frac{P_l}{P_0} = \frac{V_0}{V_l} = \frac{V_0}{V_0 - S(l - l_0)} = \frac{V_0}{V_0 + Sl_0 - Sl} \tag{6}$$

Where S represents the cross area of the cylinder, and P_l, V_l are the gas pressure and volume when the length of the vector **AB** is l, where the force generated by the cylinder is F_l.

Defining the critical length l_c as

$$l_c = \frac{V_0}{S} + l_0 \tag{7}$$

Then, the force generated by the cylinder can be written as

$$F_l = \frac{V_0F_{l_0}}{V_0 + Sl_0 - Sl} = \frac{V_0P_0S}{V_0 + Sl_0 - Sl} = \frac{C}{\frac{V_0}{S} + l_0 - l} = \frac{C}{l_c - l} \tag{8}$$

As shown in Eq. (8), it can be concluded that the relationship between the force F_l and displacement $l_c - l$ is not linear, and it is not reasonable to simplify the CBS to the liner spring.

Meanwhile, the geometric structure of the CBS is determined by four parameters a, b, h and l. The former three parameters are constants and the last parameter depends on the second joint variable θ_2.

$$l^2 = |\mathbf{AB}|^2 = b^2 + (a^2 + h^2) - 2b\sqrt{(a^2 + h^2)}\sin(\alpha - \theta_2) \tag{9}$$

Further, the angle α between the vector **AD** and **OD** can be obtained by

$$\tan\alpha = \frac{a}{h} \tag{10}$$

Then, the balance torque M applies to the second joint by the CBS is expressed as

$$M = \mathbf{F}_l \times \mathbf{BD} = \frac{C}{l(l_c - l)}b\sqrt{a^2 + h^2}\cos(\alpha - \theta_2) \tag{11}$$

Upon differentiation of Eq. (11) with respect to θ_2, it is possible to obtain the equivalent stiffness of the CBS. Thus, the practical stiffness of the second joint (comprising both the stiffness of the robot and the CBS) is defined as

$$k_2 = k_b + k_2^0 = \frac{Cb\sqrt{a^2 + h^2}\sin(\alpha - \theta_2)}{l(l_c - l)} - \frac{Cb^2(a^2 + h^2)(l_c - 2l)\cos^2(\alpha - \theta_2)}{l^3(l_c - l)^2} + k_2^0 \tag{12}$$

Here, k_b is the stiffness component of the second joint generated by the CBS, representing the influence of the CBS on the second joint stiffness, while k_2^0 is the stiffness component of the second joint without the CBS, which can be identified through the classical identification method.

From Eq. (12), it is worth noting that the stiffness of the second joint is no longer constant, which highly depends on value of joint variable θ_2, and the stiffness model of the robot with the CBS could be derived by extending the traditional stiffness model. Once the CBS is assembled in the heavy duty industrial robot (namely, the geometric parameters a, b, h are determined), k_b is determined by these two parameters C and l_c. In this case, when these two parameters are identified, the problem of stiffness with the CBS can be solved based on Eq. (12). For this reason,

one of the following sections focuses on the identification of these two parameters, so as to obtain the influence of the CBS on the stiffness of the second joint.

2.3. Joint stiffness modeling without the CBS

With the duality between the generalized relationships for motion and force transfer between the actuator and operation spaces, the relationship between the six-dimensional vector $\boldsymbol{\Gamma}$ of actuated torque and the corresponding six-dimensional vector $\mathbf{W}$ of the external load exerted on the robot EE is given by:

$$\Gamma = \mathbf{J}_f^T \mathbf{W} \tag{13}$$

Here, $\mathbf{J}_f$ is the Jacobian matrix expressed at the point where external force is applied. According to the VJM method, $\boldsymbol{\Gamma}$ can also be expressed as the function of the joint deformation vector $\Delta\boldsymbol{\theta}$ and the joint stiffness matrix $\mathbf{K}_\theta$.

$$\Gamma = \mathbf{K}_\theta \Delta\theta \tag{14}$$

The joint stiffness matrix $\mathbf{K}_\theta$ is defined as

$$\mathbf{K}_\theta = \begin{bmatrix} k_{\theta_1} & 0 & 0 & 0 & 0 & 0 \\ 0 & k_{\theta_2}^0 & 0 & 0 & 0 & 0 \\ 0 & 0 & k_{\theta_3} & 0 & 0 & 0 \\ 0 & 0 & 0 & k_{\theta_4} & 0 & 0 \\ 0 & 0 & 0 & 0 & k_{\theta_5} & 0 \\ 0 & 0 & 0 & 0 & 0 & k_{\theta_6} \end{bmatrix} \tag{15}$$

Where k_{θ_i} is the value of the ith joint stiffness. Similarly, under the linearized geometric model, the relationship between deflection $\Delta\mathbf{X}$ in the EE and the corresponding load is given by:

$$\mathbf{W} = \mathbf{K}_x \Delta\mathbf{X} = \mathbf{K}_x \mathbf{J}_m \Delta\theta \tag{16}$$

Here, $\mathbf{K}_x$ is the 6×6 matrix representing the Cartesian stiffness of the robot, and $\mathbf{J}_m$ is the Jacobian matrix expressed at the point where the position is measured. Upon differentiation of Eq. (13) with respect to $\boldsymbol{\theta}$, the relationship between $\mathbf{K}_\theta$ and $\mathbf{K}_x$ is expressed as

$$\mathbf{K}_\theta = \mathbf{K}_c + \mathbf{J}_f^T \mathbf{K}_x \mathbf{J}_m \tag{17}$$

And $\mathbf{K}_C$ is the complementary stiffness [19] defined as:

$$\mathbf{K}_c = \frac{\partial \mathbf{J}_f^T}{\partial\theta}\mathbf{W} = \left[\frac{\partial \mathbf{J}_f^T}{\partial\theta_1}\mathbf{W}, \frac{\partial \mathbf{J}_f^T}{\partial\theta_2}\mathbf{W}, \frac{\partial \mathbf{J}_f^T}{\partial\theta_3}\mathbf{W}, \frac{\partial \mathbf{J}_f^T}{\partial\theta_4}\mathbf{W}, \frac{\partial \mathbf{J}_f^T}{\partial\theta_5}\mathbf{W}, \frac{\partial \mathbf{J}_f^T}{\partial\theta_6}\mathbf{W} \right] \tag{18}$$

3. Problem of joint stiffness identification

As long as $\mathbf{J}_m$ and $\mathbf{J}_f$ are inevitable, the identification model of the joint stiffness without the CBS could be derived based on Eqs. (16) and (17).

$$\mathbf{J}_f^{-T} \mathbf{K}_\theta \mathbf{J}_m^{-1} \Delta\mathbf{X} = \mathbf{J}_f^{-T} \mathbf{K}_c \mathbf{J}_m^{-1} \Delta\mathbf{X} + \mathbf{W} \tag{19}$$

Assuming that

$$\mathbf{E} = \mathbf{J}_f^{-T} \mathbf{K}_c \mathbf{J}_m^{-1} \Delta\mathbf{X} + \mathbf{W} \tag{20}$$

From Eq. (20), it is worth noting that the matrix $\mathbf{E}$ is determined by the joint configuration $\boldsymbol{\theta}$ ($\mathbf{J}_f$ and $\mathbf{J}_m$ are the function of $\boldsymbol{\theta}$), the external load $\mathbf{W}$ and corresponding Cartesian deflection $\Delta\mathbf{X}$.

Substituting Eqs. (15) and (20) into Eq. (19), the identification model of the joint stiffness without the CBS can be rewritten in an intuitional way.

$$\begin{bmatrix} \sum_{i=1}^6 k_i \mathbf{J}_{f1i}^{-T} \mathbf{J}_{mi1}^{-1} & \sum_{i=1}^6 k_i \mathbf{J}_{f1i}^{-T} \mathbf{J}_{mi2}^{-1} & \cdots & \cdots & \sum_{i=1}^6 k_i \mathbf{J}_{f1i}^{-T} \mathbf{J}_{mi6}^{-1} \\ \sum_{i=1}^6 k_i \mathbf{J}_{f2i}^{-T} \mathbf{J}_{mi1}^{-1} & \sum_{i=1}^6 k_i \mathbf{J}_{f2i}^{-T} \mathbf{J}_{mi2}^{-1} & \cdots & \cdots & \sum_{i=1}^6 k_i \mathbf{J}_{f2i}^{-T} \mathbf{J}_{mi6}^{-1} \\ \cdots & \cdots & \cdots & \cdots & \cdots \\ \sum_{i=1}^6 k_i \mathbf{J}_{f6i}^{-T} \mathbf{J}_{mi1}^{-1} & \sum_{i=1}^6 k_i \mathbf{J}_{f6i}^{-T} \mathbf{J}_{mi2}^{-1} & \cdots & \cdots & \sum_{i=1}^6 k_i \mathbf{J}_{f6i}^{-T} \mathbf{J}_{mi6}^{-1} \end{bmatrix} \Delta\mathbf{X} = \mathbf{E} \tag{21}$$

Let the value of each joint stiffness be the component of the six-dimensional vector $\mathbf{K}$, namely,

$$\mathbf{K} = [k_1, \quad k_2^0, \quad k_3, \quad k_4, \quad k_5, \quad k_6]^T \tag{22}$$

Isolating the components of the vector $\mathbf{K}$ in Eq. (21), the identification model can be clearly expressed as

$$\mathbf{H}\mathbf{K} = \mathbf{E} \tag{23}$$

Where $\mathbf{H}$ is a 6×6 matrix as follows:

$$\mathbf{H} = \begin{bmatrix} \mathbf{J}_{f11}^{-T} \sum_{i=1}^6 \mathbf{J}_{m1i}^{-1} \Delta\boldsymbol{X}_i & \mathbf{J}_{f12}^{-T} \sum_{i=1}^6 \mathbf{J}_{m2i}^{-1} \Delta\boldsymbol{X}_i & \cdots & \cdots & \mathbf{J}_{f16}^{-T} \sum_{i=1}^6 \mathbf{J}_{m6i}^{-1} \Delta\boldsymbol{X}_i \\ \mathbf{J}_{f21}^{-T} \sum_{i=1}^6 \mathbf{J}_{m1i}^{-1} \Delta\boldsymbol{X}_i & \mathbf{J}_{f22}^{-T} \sum_{i=1}^6 \mathbf{J}_{m2i}^{-1} \Delta\boldsymbol{X}_i & \cdots & \cdots & \mathbf{J}_{f26}^{-T} \sum_{i=1}^6 \mathbf{J}_{m6i}^{-1} \Delta\boldsymbol{X}_i \\ \cdots & \cdots & \cdots & \cdots & \cdots \\ \mathbf{J}_{f61}^{-T} \sum_{i=1}^6 \mathbf{J}_{m1i}^{-1} \Delta\boldsymbol{X}_i & \mathbf{J}_{f62}^{-T} \sum_{i=1}^6 \mathbf{J}_{m2i}^{-1} \Delta\boldsymbol{X}_i & \cdots & \cdots & \mathbf{J}_{f66}^{-T} \sum_{i=1}^6 \mathbf{J}_{m6i}^{-1} \Delta\boldsymbol{X}_i \end{bmatrix} \tag{24}$$

Further, $\Delta\boldsymbol{X}_i$ is the ith component of the Cartesian deflection vector $\Delta\mathbf{X}$. With the measurement of external loads and corresponding Cartesian deflection, it is possible to compute matrixes $\mathbf{E}$ and $\mathbf{H}$. In this case, the joint stiffness could be obtained by minimizing the Euclidean norm of the approximation error ε, namely,

$$\text{minimize} \quad \varepsilon(\mathbf{K}) \equiv \frac{1}{2} \|\mathbf{H}\mathbf{K} - \mathbf{E}\|_2^2 \tag{25}$$

Nevertheless, the classical method based on the measurement of external loads and corresponding Cartesian deflection has several shortcomings. Firstly, the traditional method above requires the measurement of Cartesian deflection both in position and orientation, and three more reference points must be measured to derive the orientation deflection. While the recent measurement system such as the laser tracker, can only take the measurement of one reference point at each time. As a result, the retroreflector of the measurement system must be picked up and down in the same joint configuration, which may cause a big placement error relative to the deflection. Meanwhile, the calculation of the orientation deflection through three position measurements may lead to accumulation of measurement errors.

Usually, the vertical loading could facilitate the joint stiffness identification because the load direction can be regarded as the gravity direction. However, the vertical load cannot produce the torque in the first joint. In this case, additional experiments with non-vertical loading are required to identify the stiffness of the first joint. Nevertheless, additional measurements for the loading direction may cause some more errors, especially the placement error of the retroreflector.

Secondly, the traditional identification method for the joint stiffness identification is performed by the measurement of external force using force sensor, and the external load is assumed to be the sole factor for generating the deflection. When the robot is under no external loads, the initial joint torque before loading can be expressed by the following static equilibrium.

$$\Gamma_0 = \mathbf{G}_0 - \mathbf{f}_0 - \mathbf{M}_0 \tag{26}$$

Where $\mathbf{G}_0$ and $\mathbf{f}_0$ represent the initial gravity and static friction force before loading, respectively. And $\mathbf{M}_0 = [0, M_0, \ 0, 0, 0, 0]^T$ is the balancing torque generated by the CBS before loading.

Similarly, when the external load is applied in the EE, the current joint torque can be written as

$$\Gamma_f = \mathbf{G}_f - \mathbf{f}_f - \mathbf{M}_f + \mathbf{J}_f^T \mathbf{W} \tag{27}$$

As the joint deformation is always too small that the gravity and balancing torque before loading are almost the same as those after loading, namely, $\mathbf{G}_0$ is equal to $\mathbf{G}_f$, and $\mathbf{M}_0$ is equal to $\mathbf{M}_f$. Thus, the

toque generated by the external loads can be calculated as

$$\Gamma=\Gamma_f - \Gamma_0 = \mathbf{J}_f^T\mathbf{W} - \mathbf{f}_f + \mathbf{f}_0 \tag{28}$$

In the classical identification method, it is assumed that the static friction before loading is the same as that after loading. Under this assumption, the external load is the sole factor influencing the deflection (namely, the difference of the joint torque before and after loading is equal to $\mathbf{J}_f^T\mathbf{W}$). Practically, in the status of static equilibrium, the static friction force after loading is higher than that before loading. As a result, the real load generating the deflection is lower than the one measured from the force sensor. Thus, the final identification result of the joint stiffness using the force sensor may be higher than the real one.

Thirdly, the CBS is the important component of the heavy duty industrial robot, which has a big influence on the stiffness of the second joint (just as Eq. (12) shows). Regarding the CBS system as the spring has been proved to be unreasonable for the hydro-pneumatic system. Moreover, under the traditional identification approach, it is impossible to identify the equivalent stiffness of the CBS through the measurement of deflection and corresponding external loads: the mechanical analysis in the previous section shows that the influence of the CBS is only related to the second joint variable θ_2. Meanwhile, the joint deformation of the second joint under external loads is so small that the influence of the CBS before loading is almost the same as that after loading. In this case, the influence of the CBS on the second joint could be eliminated under these two states, before and after loading. Therefore, the equivalent stiffness of the CBS cannot be accurately identified based on the measurement of external loads and corresponding deflection before and after loading.

In a word, to accurately identify the joint stiffness of the heavy duty industrial robot with the CBS, three issues are taken into account in this paper: (1) a more thorough model and identification method for dealing with the CBS in the joint stiffness modeling and identification; (2) an efficient model for joint stiffness identification based on the measurement of position deflection rather than orientation deflection; (3) a more accurate identification approach avoiding the shortcoming of the measurement of the external load using force sensor.

4. New methodology for the joint stiffness identification

Just as the problem analysis of the joint stiffness identification above, the main attention of this section focuses on how to deal with the CBS in the second joint stiffness identification, and how to derive a more accurate identification method for the joint stiffness identification. To address the abovementioned problem, a new methodology based on the measurement of the servo motor current and position deflection is presented in this section. Firstly, the influence of the CBS on the second joint stiffness is evaluated based on the dynamic model and the motor current. Secondly, a thorough identification model is derived by the analysis of the optimal joint space for the identification. Subsequently, the joint stiffness matrix without considering the CBS is identified by the motor current and corresponding position deflection of the EE. Finally, the joint stiffness of the heavy duty industrial robot with the CBS is obtained by the combination of these two parts.

4.1. Identification of the influence of the CBS on the second joint stiffness

Compared to geometric parameters of the CBS, parameters C and l_c are largely affected by the assembling, and they can be adjusted by the initial gas volume and pressure. According to Eq. (12), the influence of the CBS on the second joint stiffness is relative to three factors: initial condition parameters C and l_c, the second joint variable θ_2. To identify the influence of the CBS on the stiffness of the second joint, this section focuses on the identification of these two initial condition parameters.

Firstly, the heavy duty industry robot is assumed to be without the CBS. Similar to the traditional robot, the joint torque of the robot can be derived by the dynamic model.

$$\tau_e = \mathbf{D}(\theta)\ddot{\theta} + \mathbf{C}(\theta, \dot{\theta}) + \mathbf{G}(\theta) + \mathbf{f}(\theta, \dot{\theta}) + \mathbf{J}_f^T(\theta)\mathbf{W} \tag{29}$$

Where $\mathbf{D}(\boldsymbol{\theta})$, $\mathbf{C}(\theta, \dot{\theta})$, $\mathbf{f}(\theta, \dot{\theta})$ and $\mathbf{G}(\boldsymbol{\theta})$ represent the inertia matrix, the centrifugal and Coriolis force vector, the friction vector, and the gravity vector, respectively; and $\mathbf{W}$ is the external force vector; $\boldsymbol{\tau}_\mathbf{e}$ is 6×1 joint torque vector without considering the CBS.

$$\tau_\mathbf{e} = [\tau_1, \tau_2^0, \tau_3, \tau_4, \tau_5, \tau_6]^T \tag{30}$$

Further, τ_i denotes the ith joint torque, τ_2^0 represents the torque of the second joint without considering the CBS. As the CBS minimizes the second joint torque, the practical torque τ_2 of the second joint is as follows

$$\tau_2 = \tau_2^0 - M \tag{31}$$

Moreover, the practical joint torque of the second joint can be measured by the corresponding servo motor current from the robot controller. Thus, the balancing torque M generated by the CBS can be derived as

$$M = \tau_2^0 - \tau_2^m \tag{32}$$

Where τ_2^m is the measured joint torque, and it can be evaluated by the motor current and corresponding current coefficients [27,28].

$$\tau_2^m = \xi_2 I_2 \tag{33}$$

Here, I_i is the measurement current of second joint servo motor. ξ_i represents the torque coefficient obtained from the datasheet of the HH-150 robot, which mainly depends on the parameters of the servo motor and RV reducer of the HH-150 robot. The detail coefficient between the joint torque and corresponding motor current can be seen in Table 2.

With the given trajectory of the robot, the second joint toque without considering the CBS (τ_2^0) can be calculated through the dynamic model. Meanwhile, the actual torque of the second joint (τ_2^m) could be measured by the motor current. Therefore, combining Eq. (11) with Eq. (32), the identification model of the CBS takes the form as

$$g(l_c, C, \theta_2) = \frac{(\tau_2^0 - \tau_2^m)l}{b\sqrt{a^2 + h^2}\cos(\alpha - \theta_2)} - \frac{C}{l_c - l} = 0 \tag{34}$$

From the identification model above, it is worth noting that the initial condition parameters (C, l_c) could be identified based on the measurement of the second motor current and dynamic model of the robot. As a result, it is possible to accurately evaluate the influence of the CBS on the second joint, so as to solve the problem of the CBS in the joint stiffness identification.

4.2. Identification of the joint stiffness without considering the CBS

As the identification problem presented in Section 3, the traditional identification model based on Eq. (25) requires to be improved to ensure the retroreflector remain unchanged in the same joint configuration. Meanwhile, the identification model should take into account the practical forces contributing to the deflection of the EE.

From Eq. (17), it can be seen that the identification would be more convenient when $\mathbf{K}_C$ is negligible with respect to $\mathbf{K}_\theta$. Under this simplification, the identification model Eq. (19) could be simplified as [20].

$$\Delta\mathbf{X} = \mathbf{J}_m \mathbf{K}_\theta^{-1} \mathbf{J}_f^T\mathbf{W} \tag{35}$$

Table 2
The coefficient between the joint torque and corresponding motor current (Nm/A).

ξ_1	ξ_2	ξ_3	ξ_4	ξ_5	ξ_6
169.6355	220.8436	220.8436	127.0724	138.3101	139.4627

Recombining the right part of the equation, and Eq. (35) can be rewritten as

$$\Delta\mathbf{X} = \begin{bmatrix} \mathbf{J}_{m11}\sum_{i=1}^{6}\mathbf{J}_{fi1}\mathrm{W}_i & \mathbf{J}_{m12}\sum_{i=1}^{6}\mathbf{J}_{fi2}\mathrm{W}_i & \cdots & \cdots & \mathbf{J}_{m16}\sum_{i=1}^{6}\mathbf{J}_{fi6}\mathrm{W}_i \\ \mathbf{J}_{m21}\sum_{i=1}^{6}\mathbf{J}_{fi1}\mathrm{W}_i & \mathbf{J}_{m22}\sum_{i=1}^{6}\mathbf{J}_{fi2}\mathrm{W}_i & \cdots & \cdots & \mathbf{J}_{m26}\sum_{i=1}^{6}\mathbf{J}_{fi6}\mathrm{W}_i \\ \cdots & \cdots & \cdots & \cdots & \cdots \\ \mathbf{J}_{m61}\sum_{i=1}^{6}\mathbf{J}_{fi1}\mathrm{W}_i & \mathbf{J}_{m62}\sum_{i=1}^{6}\mathbf{J}_{fi2}\mathrm{W}_i & \cdots & \cdots & \mathbf{J}_{m66}\sum_{i=1}^{6}\mathbf{J}_{fi6}\mathrm{W}_i \end{bmatrix}\mathbf{N} \tag{36}$$

Where W_i is the ith component of the external force vector, and $\mathbf{N}$ is the 6×1 vector, which represents the compliance value of each joint without considering the CBS.

$$\mathbf{N} = \left[\frac{1}{k_1}, \frac{1}{k_2^0}, \frac{1}{k_3}, \frac{1}{k_4}, \frac{1}{k_5}, \frac{1}{k_6}\right]^T \tag{37}$$

Considering that the external load measured by the force sensor is not the same as the practical load contributing to the deflection, the practical torque difference measured by the current instead of the force senor is used, namely

$$\sum_{i=1}^{6}\mathbf{J}_{fij}\mathrm{W}_i = \Gamma_j \tag{38}$$

Where Γ_j represents the torque difference of the jth joint before and after loading. Then, the new methodology for the joint stiffness identification takes the form as

$$\Delta\mathbf{X} = \mathbf{Q}\mathbf{N} \tag{39}$$

And

$$\mathbf{Q} = \begin{bmatrix} \mathbf{J}_{m11}\Gamma_1 & \mathbf{J}_{m12}\Gamma_2 & \cdots & \cdots & \mathbf{J}_{m16}\Gamma_6 \\ \mathbf{J}_{m21}\Gamma_1 & \mathbf{J}_{m22}\Gamma_2 & \cdots & \cdots & \mathbf{J}_{m26}\Gamma_6 \\ \cdots & \cdots & \cdots & \cdots & \cdots \\ \mathbf{J}_{m61}\Gamma_1 & \mathbf{J}_{m62}\Gamma_2 & \cdots & \cdots & \mathbf{J}_{m66}\Gamma_6 \end{bmatrix} \tag{40}$$

Compared with the traditional method Eq. (23), the proposed method Eq. (39) can be performed more conveniently and accurately by the measurement of deflection and torque difference before and after loading.

To avoid the placement error for the measurement of the orientation deflection, the joint stiffness identification can be carried out by the first three rows of matrices $\Delta\mathbf{X}$ and $\mathbf{Q}$, namely,

$$\Delta\mathbf{P} = \mathbf{L}\mathbf{N} \tag{41}$$

And

$$\mathbf{L} = \begin{bmatrix} \mathbf{J}_{m11}\Gamma_1 & \mathbf{J}_{m12}\Gamma_2 & \cdots & \cdots & \mathbf{J}_{m16}\Gamma_6 \\ \mathbf{J}_{m21}\Gamma_1 & \mathbf{J}_{m22}\Gamma_2 & \cdots & \cdots & \mathbf{J}_{m26}\Gamma_6 \\ \mathbf{J}_{m31}\Gamma_1 & \mathbf{J}_{m32}\Gamma_2 & \cdots & \cdots & \mathbf{J}_{m36}\Gamma_6 \end{bmatrix} \tag{42}$$

Where $\Delta\mathbf{P}$ represents the position deflection. In this way, only one reference point in the EE is required to get the position deflection, so that the retroreflector can be in the same place under different external loads.

However, the identification model (41) is based on the assumption that $\mathbf{K}_C$ is negligible with respect to $\mathbf{K}_\theta$. In order to identify the joint stiffness conveniently and accurately, it is necessary to analyze the influence of $\mathbf{K}_C$ on the joint stiffness identification. From Eq. (18), $\mathbf{K}_C$ is related to the joint configuration and external load on the EE. It makes sense that the higher the external load on the EE, the higher influence of $\mathbf{K}_C$ on $\mathbf{K}_\theta$. Accordingly, the worst case appears when the HH-150 robot bears the maximum external load. Let the components of the external force vector along three axes be 1500 N, and the components of the moment vector about three axes be equal to 200 Nm. For the sake of clarity, the stiffness of the first three joints is assumed to be higher than the others, and details of joint stiffness value for the analysis are in Table 3.

Because the second and third joints affect the translation motion and position significantly, the analysis about the influence of $\mathbf{K}_C$ on $\mathbf{K}_\theta$ is performed in the zones where θ_2 and θ_3 change in each joint scope, and the other four joint angles are assumed to be constant as shown in Table 4 [20].

Table 3
Arbitrary values of the joint stiffness for analysis expressed in [10^6Nm/rad].

k_1	k_2^0	k_3	k_4	k_5	k_6
1.0	1.5	2.0	0.5	0.5	0.5

Table 4
Joint configuration for analysis expressed in [°].

θ_1	θ_2	θ_3	θ_4	θ_5	θ_6
0	−40–110	−190–54	0	45	0

From Eq. (4) and the assumption above, it is possible to calculate the deflection $\Delta\mathbf{X}$ based on the given external loads and joint stiffness. In return, with the calculated $\Delta\mathbf{X}$, the joint stiffness can be identified based on the simplified identification method Eq. (41).

Finally, the relative error of the joint stiffness between the identified one and the real one (given in Table 3) are described in Fig. 4. The color in the figure illustrates the value of relative error, and the scope without color denotes that the relative error is higher than 10%. It is worth noting that the relative error in the most scope is below 5%, namely, $\mathbf{K}_C$ has little influence on the joint stiffness identification in this range. What's more, relative errors in some scope (θ_2, θ_3) are almost equal to zero.

To further obtain the joint configuration where $\mathbf{K}_C$ is negligible to the joint stiffness identification, we use the identified stiffness whose relative error is less than 5% to predict the deflection of the EE under the given worst external load.

$$\delta\mathbf{P} = \Delta\mathbf{P}_{iden} - \Delta\mathbf{P}_{real} \tag{43}$$

$$\delta\mathbf{O} = \Delta\mathbf{O}_{iden} - \Delta\mathbf{O}_{real} \tag{44}$$

Here, $\Delta\mathbf{P}_{iden}$ represents the position deflection in the EE predicted by the identified joint stiffness, and $\Delta\mathbf{P}_{real}$ is the real one calculated by given joint stiffness in Table 3. Similarly, $\Delta\mathbf{O}_{iden}$, $\Delta\mathbf{O}_{real}$ are the orientation deflection in the robot EE obtained through the identified joint stiffness and the real one, respectively.

Meanwhile, indices ε_P and ε_O are introduced to characterize the relative error of the identified joint stiffness on the deflection prediction:

$$\varepsilon_p = \frac{\|\delta\mathbf{P}\|}{\|\Delta\mathbf{P}_{real}\|} \tag{45}$$

$$\varepsilon_O = \max\{|\delta O_x|, |\delta O_y|, |\delta O_z|\} \tag{46}$$

Where δO_x, δO_y and δO_z are the orientation deflection error along the $\mathbf{x}_0$, $\mathbf{y}_0$ and $\mathbf{z}_0$ axes obtained from $\delta\mathbf{O}$, respectively.

Fig. 5 displays the maximum relative deflection error between one predicted by the identified stiffness and the real one (calculated by the given stiffness). The analysis result shows that as long as the relative error of the identified joint stiffness is less than 5%, the predicted position error of the robot EE is shown to be less than 7%. Likewise, the predicted orientation error is less than 0.0003 rad.

In other words, once the joint space (θ_2, θ_3) for stiffness identification is in an optimal zone where the relative error of the identified joint stiffness is less than 5%, $\mathbf{K}_C$ is negligible with respect to the identification of the joint stiffness. As illustrated in Fig. 6, the optimal joint configuration, where $\mathbf{K}_C$ is negligible with respect to $\mathbf{K}_\theta$, can be obtained based on the analysis results in Fig. 5.

It is worth noting that the above analysis was performed with different values of the joint stiffness than those given in Table 3. And the optimal joint configuration calculated almost remains the same, which

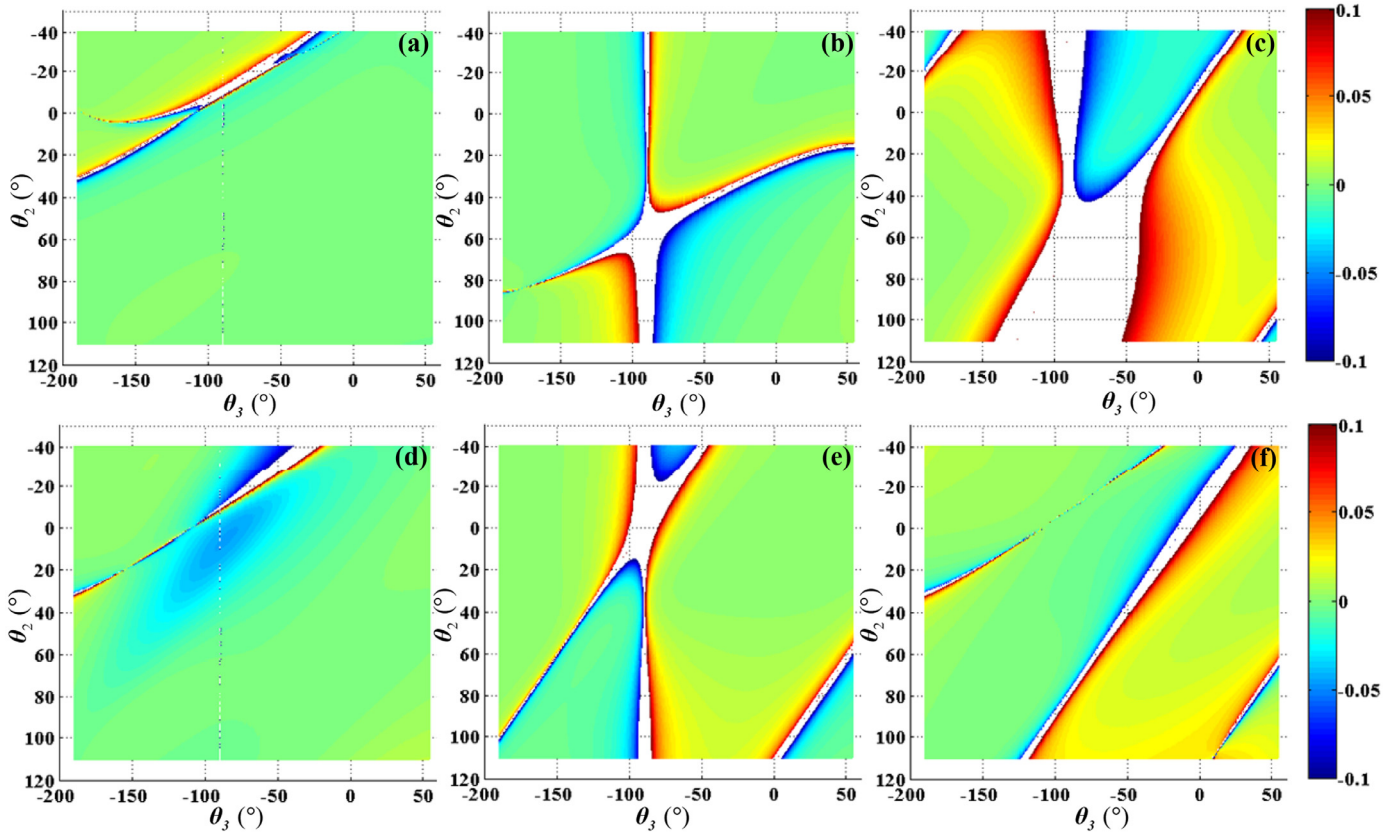

Fig. 4. The relative error of the identified joint stiffness by the proposed model in the joint space (θ_2, θ_3): (a) the relative error of the first joint stiffness; (b) the relative error of the second joint stiffness; (c) the relative error of the third joint stiffness; (d) the relative error of the fourth joint stiffness; (e) the relative error of the fifth joint stiffness; (f) the relative error of the sixth joint stiffness.

is in agreement with Dumas study [20]. Therefore, the proposed model Eq. (41) can be used to accurately identify the joint stiffness of the heavy industrial robot under the optimal joint configuration.

4.3. The methodology for the joint stiffness identification

In order to obtain the accurate joint stiffness of the heavy duty industrial robot with the CBS, a new methodology is proposed to perform the joint stiffness identification as shown in Fig. 7. As the influence of the CBS on the second joint would be eliminated under the classical method, the identification procedure is decomposed into two parts: the joint stiffness without considering the CBS and the equivalent stiffness of the CBS. And the relationship between them is described in Eq. (12): the stiffness of the second joint is highly depended on the characteristic of the CBS. In the first part, an optimal joint space (θ_2, θ_3) where $\mathbf{K}_C$ is negligible with respect to the joint stiffness identification is identified as shown in Fig. 6. Once the optimal joint space is obtained, a thorough identification model Eq. (41) is used to identify the joint stiffness based on the torque difference and position deflection. In this way, only the motor current and the position deflection are required to derive the joint stiffness. In the part of "The CBS", mechanics of the CBS is analyzed to build the equivalent stiffness model of the CBS. Then, the influence of the CBS on the second joint stiffness is identified by the dynamic model and measured motor torque of the second joint. Finally, the joint stiffness of the heavy duty industrial robot with the CBS is identified by the combination with these two parts above.

5. Experimental results and discussions

To demonstrate the effectiveness of the developed new

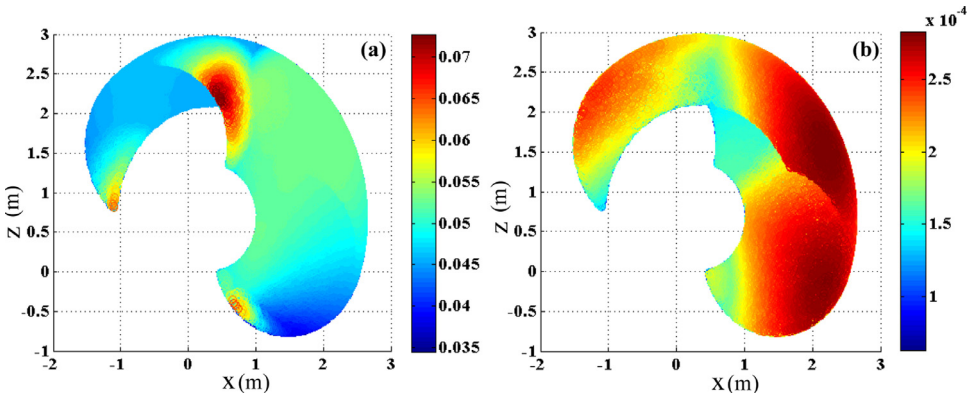

Fig. 5. The relative deflection error between the identified joint stiffness and the real one throughout the robot workspace: (a) ε_P and (b) ε_O.

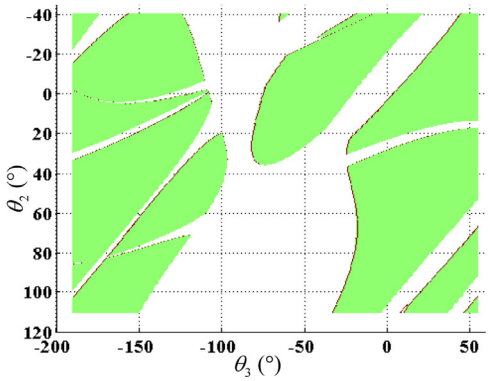

Fig. 6. The optimal joint space (θ_2, θ_3) for the joint stiffness identification by the model Eq. (41).

methodology for the joint stiffness identification of the heavy duty industrial robot with the CBS, HH-150 robot is used to carry out the identification experiment. According to the proposed identification methodology in Fig. 7, the identification experiment is performed in two steps. The first step deals with joint stiffness identification for the heavy duty industrial robot without considering the CBS. The experimental system for this identification is illustrated in Fig. 8. And the experimental setup includes the following units:

(a) 6-dof HH-150 heavy industrial robot whose kinematic parameters are calibrated in advance, and the D-H parameters of the robot are presented in Table 1;
(b) The Googol control system which provides the current measurement of each servo motor through the software ServoStudio;
(c) Special measurement tool with four reference points and loading points attached to the robot mounting flange;
(d) Laser tracker API Tracker3 with an accuracy of 10 um/m that is used to measure the Cartesian coordinates of the reference point with respect to the base frame before and after loading;
(e) Several mass blocks applied to the robot EE for generating the deflection of the robot;
(f) The force sensor that is used to measure the external load;
(g) Retroreflector that is attached to the reference point, it helps the measurement device to estimate the distances and compute the base frame for the laser tracker.

According to the optimal joint space in Fig. 6 and constraints of the experiment environment, six different joint configurations are selected to perform the identification. To avoid the placement error of the retroreflector for the measurement of the load direction, the vertical loading is applied in the former four joint configurations. On the other hand, it is impossible to identify the stiffness of the first joint by the vertical loading. Hence, the other two configurations are taken with non-vertical loading. It is worth noting that each measurement of the current and corresponding position is repeated ten times, so as to enhance the accuracy of the identification. Similarly, the average force is taken by the force sensor in every joint configuration. The details of the experiment design and data are shown in Table 5 and Fig. 9. Meanwhile, the measurement data are provided through the laser tracker whose coordinate system is located at the intersection of the first and second actuated joints: the axes Y, Z of this system are aligned with the axes of the first and second joint respectively, while the axis of X is

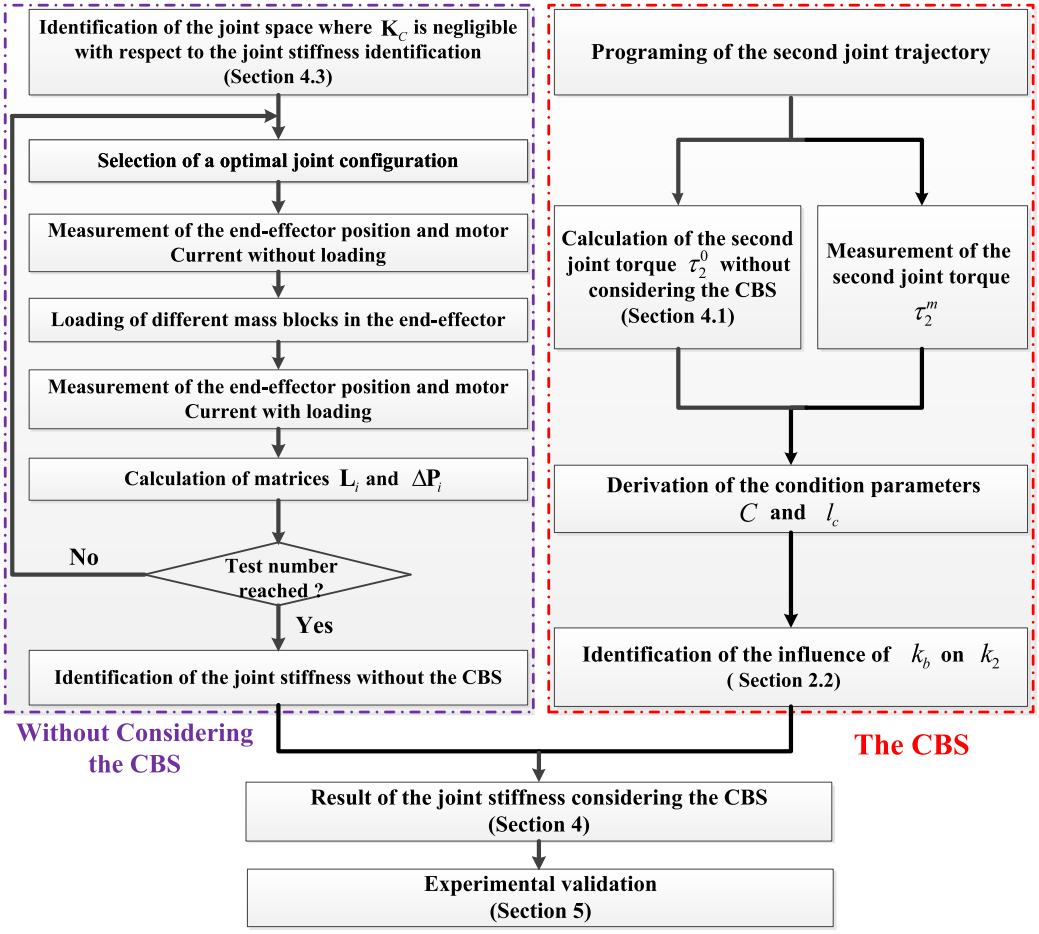

Fig. 7. Procedure for the joint stiffness identification of the heavy industrial robot with the CBS.

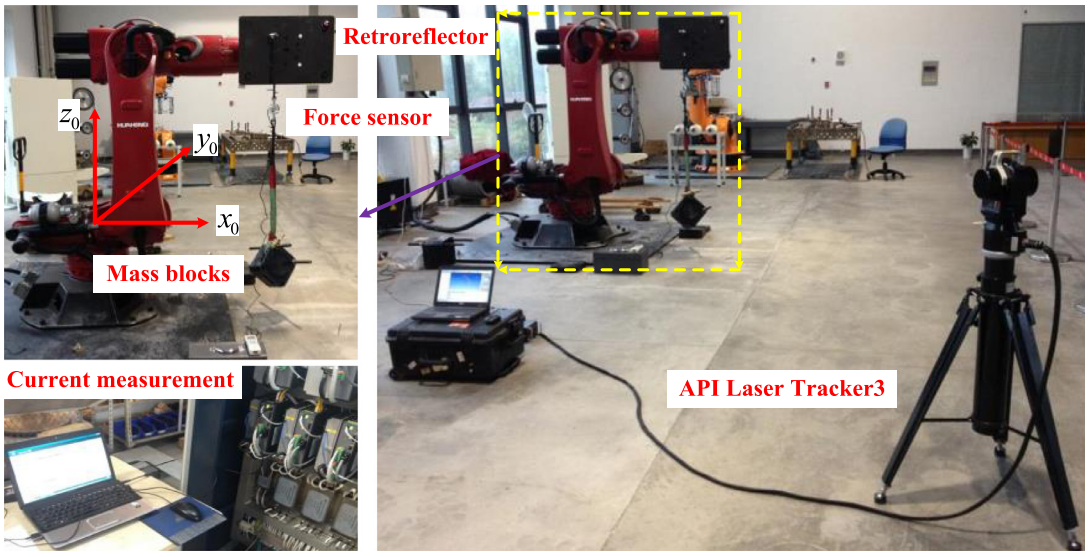

Fig. 8. The experimental setup for the joint stiffness identification.

directed base on the right-handed orthogonal basis.

With the experimental data in Table 5, it is possible to identify the joint stiffness except for the CBS based on Eq. (41). Likewise, to compare the proposed method with the traditional one, the joint stiffness is also identified by the data from force sensor and corresponding position deflection. Results of joint stiffness identified based on these two methods are presented in Table 6. It is worth noting that the stiffness of the first three joint are higher than the other three ones, which is accordance with the design of the heavy duty industrial robot. Furthermore, there are some differences among these two methods for the joint stiffness identification: the stiffness identified by the force sensor is higher than the one identified by the proposed method. As the experiment of each configuration is repeated ten times, the noise error of the measurement could be eliminated largely. Thus, the main reasons for these differences can be explained as: (1) in the former four joint configurations, the direction of external load can be treated as the vertical direction, and it does not require any measurement of the load direction. In the last two configurations, the traditional identification method requires to measure the direction of the external load by the laser tracker, which would result in placement error of the retroreflector for the deflection measurement. Whereas, the proposed method is performed by the measurement of the current difference without the measurement of load direction; (2) just as the problem states in Section 3, the traditional identification method is based on the assumption that the deflection is only attributed to the external load measured by the force sensor. In practice, the static friction force after loading is higher than the one before loading. In this case, the difference of the static friction force would lead the practical load lower than the measurement value from the force sensor. Thus, the matrix **L** in the model Eq. (41) is larger than the real one. In return, the compliance matrix **N** will be lower than practical one. Therefore, the joint stiffness identified based on the force sensor is higher than the one identified by the proposed method, which matches better with the problem analysis in Section 3. Moreover, to further validate the accuracy of the proposed methodology, the validation experiment is carried out in Section 6.

As the influence of the CBS is eliminated in the first step, the second

Table 5
The experiment data for the joint stiffness identification.

Configuration	External force (F_x, F_y, F_z) (N)	Current measured (I_1, I_2...I_6) (A)	Deflection measured (δ_x, δ_y, δ_z) (mm)
1	(0, 0, 0)	(-0.15, 3.22, 8.16, -2.03, -0.48, 0.23)	–
	(0, 0, 467)	(-0.13, 6.40, 9.76, -2.71, -0.47, 0.52)	(0.5544, -0.1564, -1.1377)
	(0, 0, 641)	(-0.12, 7.42, 10.31, -3.02, -0.45, 0.62)	(0.7752, -0.2472, -1.5545)
	(0, 0, 814)	(-0.13, 8.62, 10.91, -3.37, -0.49, 0.73)	(0.9838, -0.3252, -2.0010)
	(0, 0, 1078)	(-0.13, 10.28, 11.79, -3.96, -0.50, 0.90)	(1.3219, -0.3607, -2.6608)
2	(0, 0, 0)	(-0.12, 6.88, 7.56, 0.96, 2.39, -0.11)	–
	(0, 0, 467)	(-0.13, 8.30, 9.67, 0.47, 2.79, 0.10)	(0.4556, -0.1713, -0.9005)
	(0, 0, 642)	(-0.12, 8.52, 10.55, 0.36, 3.08, 0.24)	(0.7087, -0.2270, -1.2675)
	(0, 0, 816)	(-0.11, 9.80, 11.45, 0.24, 3.42, 0.36)	(0.9238, -0.4178, -1.6395)
	(0, 0, 990)	(-0.12, 9.87, 12.32, 0.11, 3.73, 0.47)	(1.1791, -0.4451, -2.0159)
3	(0, 0, 0)	(-0.11, 4.90, 8.90, 0.15, -0.33, 0.23)	–
	(0, 0, 466)	(-0.11, 7.86, 11.55, 0.09, 0.47, 0.42)	(1.0275, -0.2534, -1.4475)
	(0, 0, 641)	(-0.12, 8.71, 12.09, 0.09, 0.96, 0.52)	(1.4041, -0.2935, -1.9292)
	(0, 0, 815)	(-0.12, 9.75, 13.02, 0.05, 1.40, 0.65)	(1.7456, -0.3119, -2.4201)
	(0, 0, 989)	(-0.10, 11.00, 13.90, 0.03, 1.89, 0.74)	(2.0971, -0.3650, -2.8930)
4	(0, 0, 0)	(-0.11, 6.40, 5.20, -2.03, -1.24, 0.11)	–
	(0, 0, 466	(-0.11, 8.24, 7.21, -2.69, -1.26, 0.37)	(0.3473, -0.1729, -0.6294)
	(0, 0, 640)	(-0.11, 8.72, 7.80, -3.03, -1.26, 0.49)	(0.4866, -0.2268, -0.8821)
	(0, 0, 813)	(-0.10, 9.33, 8.52, -3.38, -1.27, 0.60)	(0.6341, -0.2704, -1.1457)
	(0, 0, 988)	(-0.11, 9.95, 8.78, -3.78, -1.27, 0.71)	(0.7948, -0.3102, -1.4020)
5	(0, 0, 0)	(0.26, 6.70, 7.15, 0.93, 2.04, -0.26)	–
	(175, −763, −896)	(8.01, 8.40, 9.77, 1.80, 2.86, -0.24)	(0.0378, -2.9139, -1.1052)
6	(0, 0, 0)	(-0.22, 6.13, 5.48, 0.93, 2.00, -0.22)	–
	(−374, −985, −580)	(6.42, 7.92, 7.82, 2.09, 2.21, -0.52)	(-0.7133, -2.8566, -0.9588)

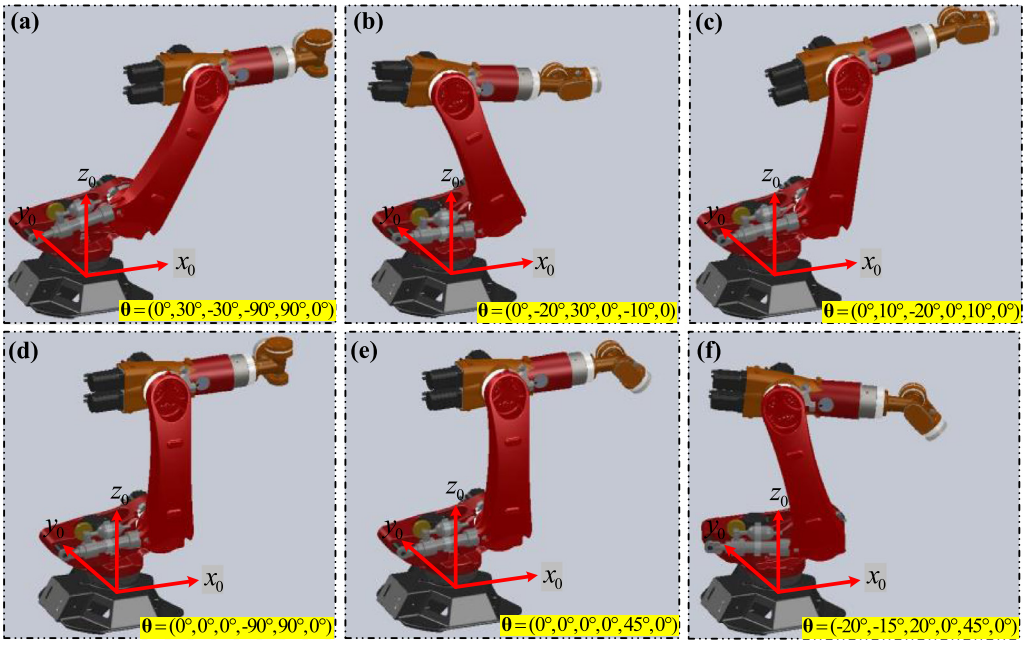

Fig. 9. The robot configuration for the stiffness identification: (a) the first configuration; (b) the second configuration; (c) the third configuration; (d) the forth configuration; (e) the fifth configuration; and (f) the sixth configuration.

Table 6
Identified results of the joint stiffness by two different methods expressed in [10^6 Nm/rad].

Identified method	k_1	k_2^0	k_3	k_4	k_5	k_6
Current	0.559	1.435	1.829	0.184	0.171	0.070
Force	0.708	1.607	2.602	0.221	0.235	0.085

step is devoted to identifying the influence of the CBS on the second joint stiffness. Two different external loads as illustrated in Fig. 10 are used to obtain the relationship between M and θ_2. Just as Table 7 shows, let the second joint rotate with the given angular velocity from A_1 to A_2, while the other five joints remain stationary in the given configuration. Meanwhile, the current of the second motor are measured from the robot controller. As a result, torques of the second joint under different angular velocities and loads are obtained through the measured current. Then, the balancing torque M generated by the CBS can be calculated based on Eq. (32). It is worth noting that the friction torque with the given joint trajectory has been measured in advance, and the details about how to obtain the influence of the friction torque is illustrated in Section 6.

Similar to the analysis of the CBS in Section 2.2, the result in Fig. 11 shows that the balancing torque M only depends on the joint variable θ_2, and the maximum relative error between different angular velocity

Table 7
Joint configuration for the CBS identification [°].

θ_1	θ_2	θ_3	θ_4	θ_5	θ_6
0	−20–40	0	0	90	0

and loads is less than 5%. It is worth noting that when the position of the second joint is about 3.3°, the balancing torque is close to zero, which is in a good agreement with the mechanical analysis of the CBS.

Subsequently, with the result of the balancing torque above, the initial condition parameters of the CBS can be identified based on Eq. (34).

$$\begin{cases} C = 4771.4 \text{ Nm} \\ l_c = 0.9112 \text{ m} \end{cases} \tag{47}$$

Meanwhile, to validate the accuracy of the identified initial condition parameters, the new experiment is carried out with different joint angular velocity and rotation scope. Then, the numerical result of the balancing torque is calculated based on the identified initial condition parameters. The comparison of the balancing torque between the experiment and numerical result is illustrated in Fig. 12. It makes sense that the numerical result matches well with the experiment, and the maximum relative error between them is less than 7%.

Finally, the influence of the CBS on the second joint stiffness is

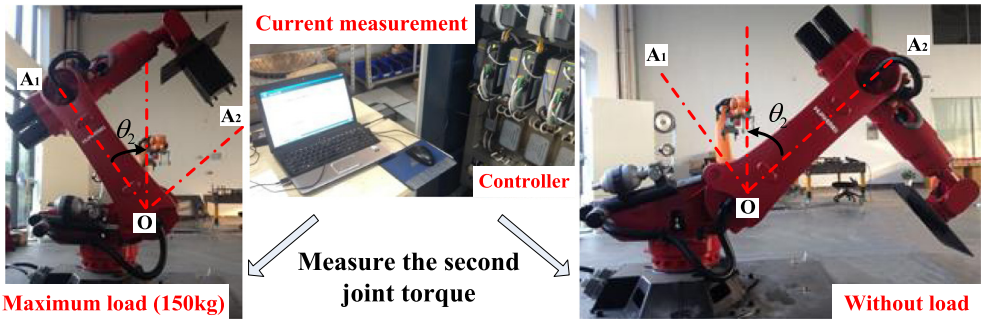

Fig. 10. The experimental setup for the identification of the CBS.

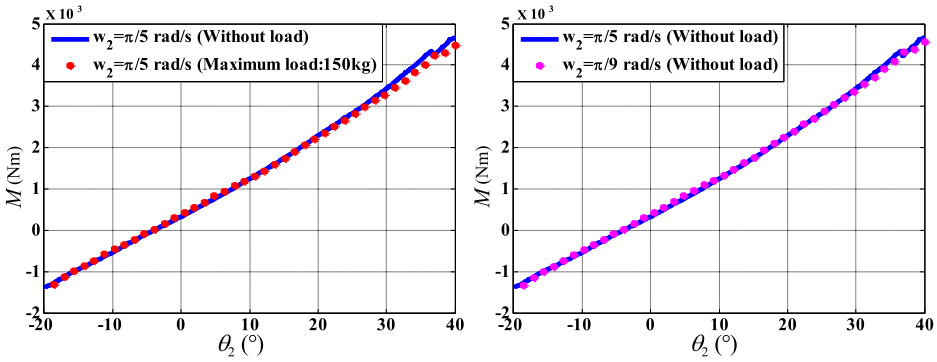

Fig. 11. The relation between θ_2 and M under different loads and angular velocities.

derived in Fig. 13(a). Combining with two identification steps above, the second joint stiffness of the robot with the CBS is illustrated in Fig. 13(b). In contrast to the traditional industrial robot without the CBS, the value of k_2 is no longer a constant but a function of the second joint variable θ_2. Furthermore, the CBS has a larger influence on k_2 with the increase of the second joint variable θ_2, which is helpful for the robotic workspace optimization during the manufacturing process.

6. Experimental validation

To further verify the accuracy of the proposed identification methodology for the joint stiffness identification based on the current, a validation experiment is carried out in this section. As illustrated in Fig. 14 and Table 8, a linear trajectory **UV** with a low speed motion instead of static position is used to analyze the position deflection of the EE: usually, it is hard to derive the practical load contributing to the joint deformation when the robot is in the status of static equilibrium, as it is difficult to obtain the accurate model of the static friction. While the friction torque of the trajectory with a low speed could be conveniently obtained by the experiment. Moreover, when the robot is under the low speed motion, the dynamic force is almost zero, and it can be regarded as a quasi-static process. Therefore, the low speed motion is chosen for the validation experiment, so as to accurately predict the position deflection by considering the influence of the friction.

In order to obtain the friction torque of the given trajectory, an experiment is performed in advance. Firstly, motor currents are measured as the robot moves along the designed trajectory **UV**. Similarly, when the robot moves along the opposite trajectory (trajectory **VU**), motor currents are measured under the same condition. In this case, the influence of friction on the motor torque can be obtained by the difference between those two measurements.

As shown in Fig. 15, the third motor is taken as an example to illustrate the way to obtain the friction torque. It is noteworthy that the measured motor current on the trajectory **UV** is higher than that on the trajectory **VU**: When the robot moves along the trajectory **UV**, the third joint rotates in the negative direction, where the direction of friction matches with that of the external payload. In turn, when the third joint moves along the trajectory **VU**, the opposite friction would help to balance the external payload. As a result, the motor current in the trajectory **UV** is bigger than that in the trajectory **VU**. Meanwhile, there exists twice friction difference between these two different trajectories. Thus, the equivalent friction torque (current) of the third joint can be calculated as follows:

$$I_{f3} = \frac{1}{2}|I_{UV3} - I_{VU3}| \tag{48}$$

Where I_{f3} represents the equivalent friction torque (current) of the third joint. I_{UV3} represents the third motor current along the trajectory **UV**. I_{VU3} represents the third motor current along the trajectory **VU**.

Similarly, the influence of friction on other motor currents during the given trajectory could be derived in the same way. Taking into account the friction effects, it is possible to predict the position deflection based on the identified joint stiffness and practical load. Meanwhile, the real position deflection of the reference point is measured by the laser tracker.

Comparisons of position deflection between the experiment and two predictive values (that is, predicted by identification stiffness through the force sensor and current, respectively) are presented in Fig. 16. It is worth noting that the position deflection predicted based on the proposed method matches better with the experiment: just as the analysis of identify problem in Sections 3 and 4.2, the joint stiffness identified by the force sensor is higher than the real one. Thus, the corresponding predictive value of the position deflection would be lower than the one predicted by the proposed method, and values of position errors predicted by the proposed method are much closer to the experiment measurement.

In addition, with the identified join stiffness, it is able to calculate the joint deformation $\Delta\boldsymbol{\theta}$ along the given trajectory **UV.** Usually, the joint deformation is so small that it is plausible to assume the stiffness

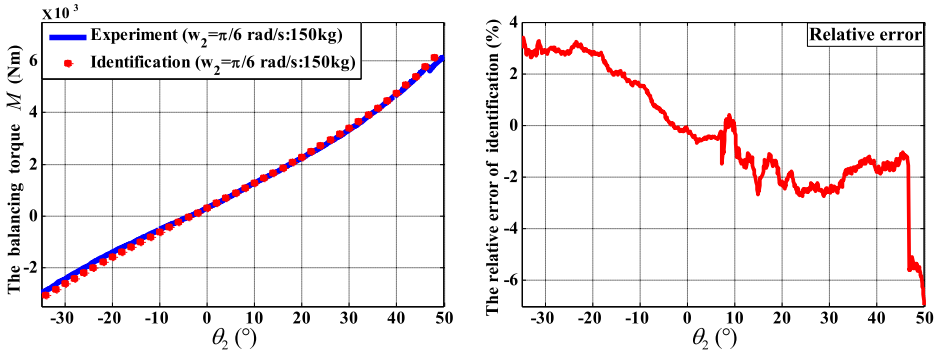

Fig. 12. The comparison of the balancing torque between the experiment and the numerical result.

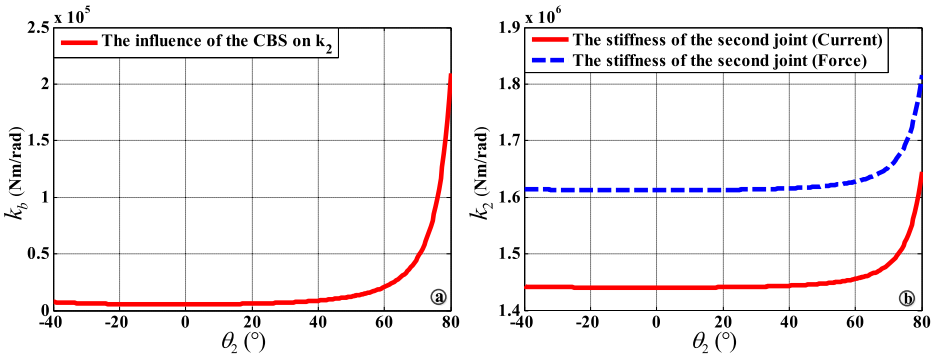

Fig. 13. The stiffness of the second joint: (a) the influence of the CBS on k_2, and (b) the second joint stiffness of the heavy duty industrial robot with the CBS.

of the EE before deformation is the same as that after deformation. Consequently, we can compensate the joint compliance by subtracting the joint deformation $\Delta\boldsymbol{\theta}$ from the original joint configuration along the given trajectory. In this way, trajectory position errors of the given trajectory **UV** are measured when the robot is compensated by the identified joint stiffness with two different methods. The comparison result of the trajectory position error is presented in Fig. 17. It can be seen that the trajectory position accuracy has been improved after compensation by both two identified methods, although there still exists some position errors, which can be explained by errors of the kinematic parameters and the base frame construction of the tracker system.

Meanwhile, for the trajectory performance in the X direction, there exists no significant difference between these two identified methods. Nevertheless, the position error in the Z direction has been largely reduced after compensation by the proposed method compared to that one by the force sensor. Therefore, with comparison results from the position deflection prediction and the trajectory performance, the proposed method based on the current is tested to be able to identify the joint stiffness, and the future focus will be paid to the trajectory optimization and error compensation based on the identified joint stiffness.

7. Conclusion

This paper presents a new methodology for the joint stiffness identification of the heavy industrial robot with the CBS, which is important for the workspace optimization and deflection compensation in the robotic machining. The main contribution of this study is the novel thorough stiffness modeling and corresponding identification method for the heavy duty industrial robot with the CBS: 1) thorough stiffness modeling and identification approach for dealing with the hydro-pneumatic CBS in the heavy duty industrial robot; 2) a more accurate methodology for the joint stiffness identification.

Firstly, the mechanism of the CBS is analyzed theoretically, and the influence of the CBS on the second joint stiffness is derived in a rational way, which reflects the clear physical meanings of the CBS. Meanwhile, the equivalent stiffness of the CBS is identified by the dynamic model and measurement of the second joint torque. The result shows that the CBS has a larger effect on the second joint stiffness with the increase of the joint variable θ_2.

Secondly, with the analysis of the present identification approach, a new methodology for the joint stiffness identification is proposed in this study, which is based on the measurement of the servo current and corresponding position deflection. In contrast to the traditional identification method, the main advantages of the proposed methodology are:

Table 8
The trajectory of the robot for the validation experiment.

The trajectory of the robot	The velocity and external load of the trajectory
x_U = 1200 mm y_U = 0 mm z_U = 116 mm x_V = 1800 mm y_V = 0 mm z_V = 116 mm	v_x = 10 mm/s W = 1500 N

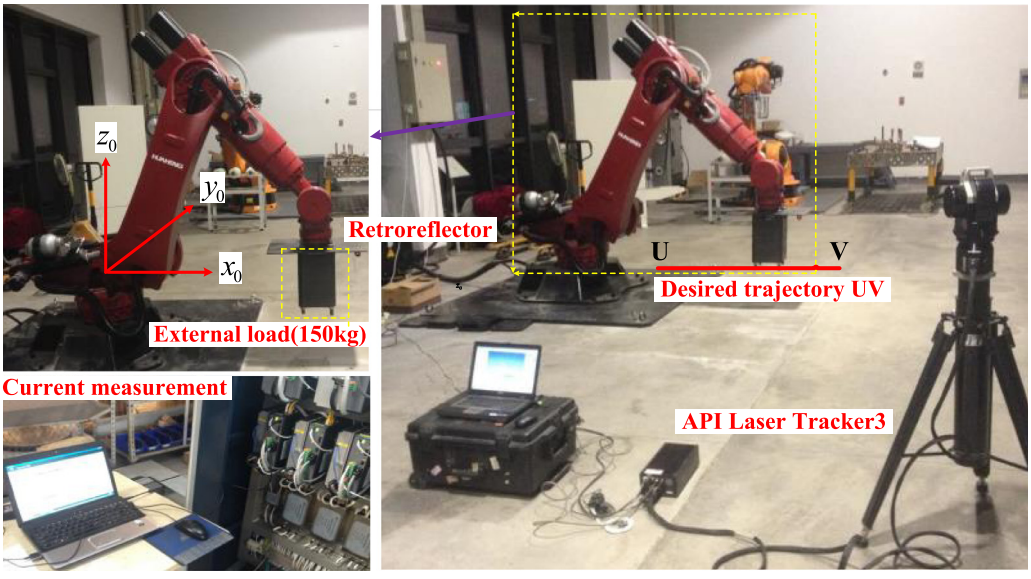

Fig. 14. The experimental setup for the validation of proposed methodology.

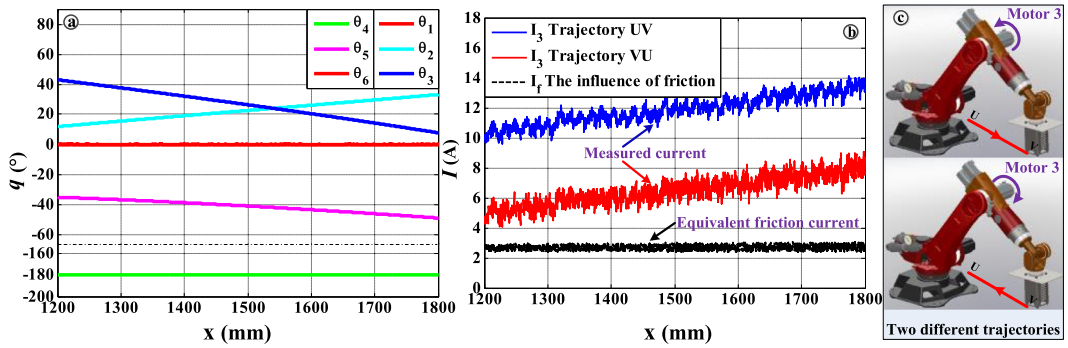

Fig. 15. The friction torque with the given trajectory: (a) the joint trajectory along the trajectory UV; (b) the influence of the friction on the motor torque; and (c) two different trajectories.

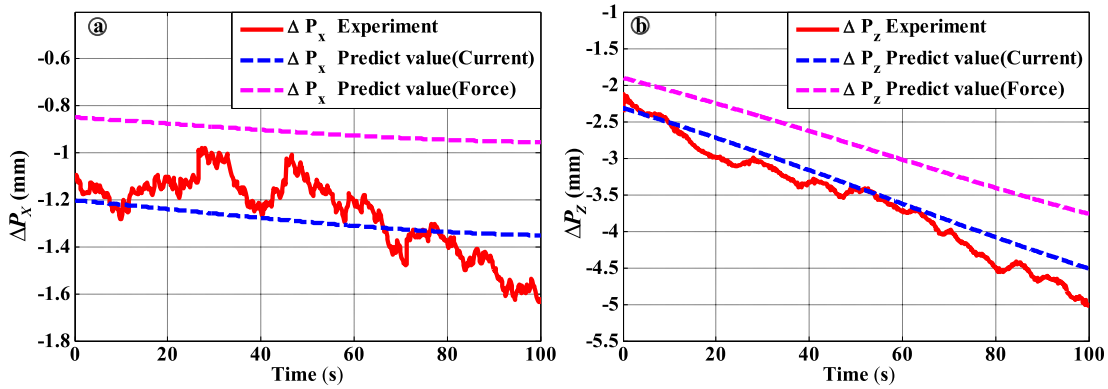

Fig. 16. The comparison of the position deflection prediction among different methods: (a) the position deflection in the X direction evaluated by experiment, stiffness identified through the current and the force sensor; (b) the position error in the Z direction evaluated by the above three methods.

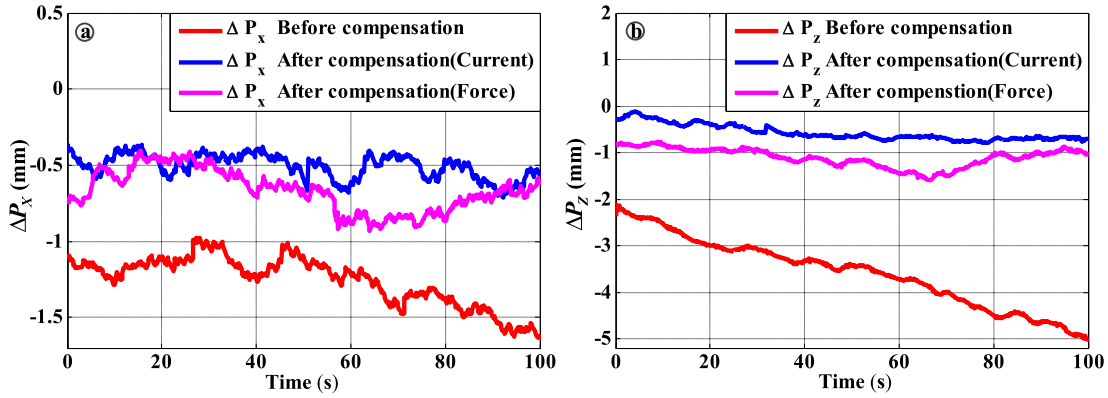

Fig. 17. The comparison of the trajectory position errors among different situations: (a) the position error in the X direction before compensation, after compensation by the identified joint stiffness with the current, and after compensation by the identified joint stiffness with the force sensor; and (b) the position error in the Z direction before compensation, after compensation by the identified joint stiffness with the current, and after compensation by the identified joint stiffness with the force sensor.

1) it only requires the measurement of the position deflection in the reference point, avoiding the placement error of the retroreflector; 2) the current measured from the controller can reflect the practical loads accounting for the deflection, which considers the friction difference before and after loading; 3) the proposed approach is performed by the measurement of the current difference without measuring the direction of the external load, which can avoid the placement error of the retroreflector.

Finally, combing with two identification steps above, an experiment is performed to identify the joint stiffness of HH-150 robot. It is worth noting that the joint stiffness identified by the force sensor is higher than the one identified by the proposed method, which is in a good agreement with the problem analysis in Section 3. To further verify the proposed method, a new validation experiment is carried out in the Section 6. The result shows that the proposed method is able to identify the joint stiffness of the heavy duty industrial robot with the CBS, which further demonstrates the proposed method outperforms in terms of: 1) accuracy of the identification result; 2) convenience in designing the identification scheme; 3) efficiency in implementing the identification.

In general, the proposed method for the stiffness identification is showed to be able to deal with the CBS of the heavy duty industrial robot. However, there exist some limitations for further improving the identification accuracy in the future: (1) the equivalent stiffness modeling is based on the kinematics of the CBS without considering its dynamics in the super speed motion; (2) the stiffness model neglects the influence of the compliance of link; (3) the identification experiment requires constructing the base coordinate for the deflection measurement, which may affect the identification accuracy.

Acknowledgments

This work is supported by the Major State Basic Research Development Program of China (973 Program, Grant no. 2014CB046704), National Science and Technology Support Plan (Grant no. 2014BAB13B01).

References

[1] S. Yixu, L. Hongbo, Y. Zehong, An adaptive modeling method for a robot belt grinding process, IEEE/ASME Trans. Mechatron. 17 (2) (2012) 309–317.
[2] Y. Guo, H. Dong, Y. Ke, Vibration analysis and suppression in robotic boring process, Int. J. Mach. Tools Manuf. 101 (2016) 102–110.
[3] J. Belchior, M. Guillo, E. Courteille, Off-line compensation of the tool path deviations on robotic machining: Application to incremental sheet forming, Robot. Comput.-Integr. Manuf. 29 (4) (2013) 58–69.
[4] S. Zivanovic, N. Slavkovic, D. Milutinovic, An approach for applying STEP-NC in robot machining, Robot. Comput.-Integr. Manuf. 49 (2018) 361–373.
[5] M. Guillo, L. Dubourg, Impact & improvement of tool deviation in friction stir welding: Weld quality & real-time compensation on an industrial robot, Robot. Comput.-Integr. Manuf. 39 (2016) 22–31.
[6] Y. Lin, H. Zhao, H. Ding, Posture optimization methodology of 6R industrial robots for machining using performance evaluation indexes, Robot. Comput.-Integr. Manuf. 48 (2017) 59–72.
[7] J. De Backer, A. Christiansson, Investigation of path compensation methods for robotic friction stir welding, Ind. Robot: Int. J. 39 (6) (2012) 601–608.
[8] A. Klimchik, A. Ambieh, S. Garnier, Efficiency evaluation of robots in machining applications using industrial performance measure, Robot. Comput.-Integr. Manuf. 48 (2017) 12–29.
[9] A. Klimchik, B. Furet, S. Caro, Identification of the manipulator stiffness model parameters in industrial environment, Mech. Mach. Theory 90 (2015) 1–22.
[10] D. Deblaise, X. Hernot, P. Maurine, A systematic analytical method for PKM stiffness matrix calculation, Proceedings of the 2006 IEEE International Conference on Robotics and Automation, Orlando, Florida, USA, 2006, pp. 4213–4219.
[11] G. Piras, W.L. Cleghorn, J.K. Mills, Dynamic finite-element analysis of a planar high-speed, high-precision parallel manipulator with flexible links, Mech. Mach. Theory 40 (7) (2005) 849–862.
[12] A. Klimchik, A. Pashkevich, D. Chablat, CAD-based approach for identification of elasto-static parameters of robotic manipulators, Finite Elem. Anal. Des. 75 (2013) 19–30.
[13] G. Ecorchard, R. Neugebauer, P. Maurine, Elasto-geometrical modeling and calibration of redundantly actuated PKMs, Mech. Mach. Theory 45 (5) (2010) 795–810.
[14] A. Bres, B. Monsarrat, L. Dubourg, Simulation of friction stir welding using industrial robots, Ind. Robot: Int. J. 37 (1) (2010) 36–50.
[15] E. Abele, J. Bauer, T. Hemker, Comparison and validation of implementations of a flexible joint multibody dynamics system model for an industrial robot, CIRP J. Manuf. Sci. Technol. 4 (1) (2011) 38–43.
[16] J.K. Salisbury, Active stiffness control of a manipulator in Cartesian coordinates, 19th IEEE Conference on Decision and Control Including the Symposium on Adaptive Processes, 1980, pp. 95–100.
[17] C. Gosselin, Stiffness mapping for parallel manipulators, IEEE Trans. Robot. Autom. 6 (3) (1990) 377–382.
[18] S. Chen, I. Kao, Conservative congruence transformation for joint and Cartesian stiffness matrices of robotic hands and fingers, Int. J. Robots Res. 19 (9) (2000) 835–847.
[19] G. Alici, B. Shirinzadeh, Enhanced stiffness modeling, identification and characterization for robot manipulators, IEEE Trans. Robot. 21 (4) (2005) 554–564.
[20] C. Dumas, B. Furet, S. Caro, Joint stiffness identification of six-revolute industrial serial robots, Comput.-Integr. Manuf. 27 (4) (2011) 881–888.
[21] C. Dumas, B. Furet, S. Caro, Joint stiffness identification of industrial serial robots, Robotica 30 (04) (2012) 649–659.
[22] A. Klimchik, Y. Wu, C. Dumas, Identification of geometrical and elastostatic parameters of heavy industrial robots, Robotics and Automation (ICRA), 2013 IEEE International Conference on, 2013, pp. 3707–3714.
[23] A. Klimchik, E. Magid, A. Pashkevich, Design of experiments for elastostatic calibration of heavy industrial robots with kinematic parallelogram and gravity compensator, IFAC. 49(12) (2016) 967–972.
[24] B. Siciliano, O. Khatib, Springer Handbook of Robotics, Springer, Berlin, Germany, 2016.
[25] J.J. Craig, Introduction to Robotics: Mechanics and Control, Addison-Wesley, 2005.
[26] J. Angeles, J. Angeles, Fundamentals of Robotic Mechanical Systems, Springer, 2002.
[27] W. Khalil, E Dombre, M Nagurka, Modeling, identification and control of robots, Hermes Penton Sci. (2004).
[28] A. Calanca, L.M. Capisani, A. Ferrara, L. Magnani, MIMO closed loop identification of an industrial robot, IEEE Trans. Control Syst. Technol. 19 (5) (2011) 1214–1224.